








# Do LIGO/Virgo Black Hole Mergers Produce AGN Flares? The Case of GW190521 and Prospects for Reaching a Confident Association

A. Palmese<sup>1,2</sup> , M. Fishbach<sup>3,6</sup> , C. J. Burke<sup>4,5</sup> , J. Annis<sup>1</sup> , and X. Liu<sup>4,5</sup> 

<sup>1</sup>Fermi National Accelerator Laboratory, P.O. Box 500, Batavia, IL 60510, USA; [palmese@fnal.gov](mailto:palmese@fnal.gov)

<sup>2</sup>Kavli Institute for Cosmological Physics, University of Chicago, Chicago, IL 60637, USA

<sup>3</sup>Center for Interdisciplinary Exploration and Research in Astrophysics (CIERA) and Department of Physics and Astronomy, Northwestern University, 1800 Sherman Avenue, Evanston, IL 60201, USA

<sup>4</sup>Department of Astronomy, University of Illinois at Urbana-Champaign, Urbana, IL 61801, USA

<sup>5</sup>National Center for Supercomputing Applications, University of Illinois at Urbana-Champaign, Urbana, IL 61801, USA

Received 2021 March 30; revised 2021 June 3; accepted 2021 June 5; published 2021 June 21

## Abstract

The recent report of an association of the gravitational-wave (GW) binary black hole (BBH) merger GW190521 with a flare in the active galactic nuclei (AGNs) J124942.3 + 344929 has generated tremendous excitement. However, GW190521 has one of the largest localization volumes among all of the GW events detected so far. The 90% localization volume likely contains 7400 unobscured AGNs brighter than  $g \leq 20.5$  AB mag, and it results in a  $\gtrsim 70\%$  probability of chance coincidence for an AGN flare consistent with the GW event. We present a Bayesian formalism to estimate the confidence of an AGN association by analyzing a population of BBH events with dedicated follow-up observations. Depending on the fraction of BBHs arising from AGNs, counterpart searches of  $\mathcal{O}(1) - \mathcal{O}(100)$  GW events are needed to establish a confident association, and more than an order of magnitude more for searches without follow-up (i.e., using only the locations of AGN and GW events). Follow-up campaigns of the top  $\sim 5\%$  (based on volume localization and binary mass) of BBH events with total rest-frame mass  $\geq 50 M_{\odot}$  are expected to establish a confident association during the next LIGO/Virgo/KAGRA observing run (O4), as long as the true value of the fraction of BBHs giving rise to AGN flares is  $> 0.1$ . Our formalism allows us to jointly infer cosmological parameters from a sample of BBH events that include chance coincidence flares. Until the confidence of AGN associations is established, the probability of chance coincidence must be taken into account to avoid biasing astrophysical and cosmological constraints.

*Unified Astronomy Thesaurus concepts:* [Gravitational wave astronomy \(675\)](#); [Gravitational wave sources \(677\)](#); [Gravitational waves \(678\)](#); [Cosmology \(343\)](#); [Active galactic nuclei \(16\)](#); [Transient sources \(1851\)](#); [High energy astrophysics \(739\)](#); [Time domain astronomy \(2109\)](#)

## 1. Introduction

One of the most interesting gravitational-wave (GW) detections to date is the binary black hole (BBH) merger GW190521 (Abbott et al. 2020b). This event is associated with the most massive binary system detected by LIGO/Virgo so far, with a total mass of  $\sim 150 M_{\odot}$ . This makes GW190521 particularly interesting, since the origin of black holes in the mass gap challenges the standard theories of stellar evolution (Abbott et al. 2020e), although the origin of this event as an isolated binary cannot be excluded (Farrell et al. 2020; Kinugawa et al. 2020), and the component mass may fall outside of the mass gap (Fishbach & Holz 2020). This detection therefore resulted in a large number of proposed alternative formation scenarios including primordial black holes (Luca et al. 2020), exotic Proca stars (Bustillo et al. 2021), low-mass dwarf galaxy mergers (Conselice et al. 2020; Palmese & Conselice 2021), dynamical interactions in dense stellar environments (Romero-Shaw et al. 2020; Gayathri et al. 2020a; Fragione et al. 2020), and black holes grown by accretion (Safarzadeh & Haiman 2020). The latter scenario can also occur in active galactic nuclei (AGNs) disks, although the accretion probably happens at a relatively low rate, affecting BH masses by  $\lesssim 10\%$  (Tagawa et al. 2020; Yang et al. 2020). A compelling explanation for the formation of massive stellar black holes is through repeated mergers of smaller black holes (Fishbach et al. 2017; Gerosa & Berti 2017), and such hierarchical mergers are a natural

prediction for BBHs assembled in AGN disks (McKernan et al. 2012, 2014; Yang et al. 2019). Because of the gas-rich environment, BBH mergers in AGN disks may also give rise to electromagnetic counterparts through several mechanisms (e.g., McKernan et al. 2012; Bartos et al. 2017b; McKernan et al. 2019; Kimura et al. 2021). This is particularly relevant for GW190521 because Graham et al. (2020, hereafter G20) found a potential electromagnetic (EM) counterpart in AGN J124942.3 + 344929 using Zwicky Transient Facility (ZTF; Masci et al. 2018; Bellm et al. 2018) observations.

The prospect of EM counterparts to BBH events is exciting for several reasons, including the potential for standard siren cosmology (Schutz 1986; Holz & Hughes 2005; Chen et al. 2018; Palmese et al. 2019). GW events have already been used to independently measure the Hubble constant (Abbott et al. 2017a; Fishbach et al. 2018; Abbott et al. 2019; Soares-Santos & Palmese et al. 2019; Palmese et al. 2020). Meanwhile, the AGN association with GW190521 has also been used in several works to derive cosmological constraints (Chen et al. 2020; Gayathri et al. 2020b; Mukherjee et al. 2020; Haster 2020). However, these analyses do not account for the probability of a chance coincidence, which is particularly significant because GW190521 has the second largest localization in terms of comoving volume encompassed among all GW detection so far (see Table 1 for the volume of a selected sample of LIGO/Virgo events). Moreover, De Paolis et al. (2020) suggest that this AGN flare may also be explained by a microlensing event.

<sup>6</sup> NASA Hubble Fellowship Program Einstein Postdoctoral Fellow.

**Table 1**

Comoving Volume (99% CI) for the Sample of LIGO/Virgo GW Binary Black Hole Events Considered in This Work

Event	Volume (Gpc <sup>3</sup> )
GW190814	$9.2 \times 10^{-5}$
GW170814	$1.5 \times 10^{-4}$
GW190701_203306	0.087
GW190521	9.1

**Note.** Notice that GW190521 has a volume orders of magnitude larger than the other events.

In this work, we expand on the analysis presented in Ashton et al. (2020) and find insufficient evidence for a common origin for GW190521 and the AGN flare. We explore the uniqueness of the candidate and the odds of chance coincidence for similar flares based on the population of AGNs expected in the entire and observed GW190521 localization volumes. We then turn to a population of GW events with possible AGN counterparts, and define a Bayesian formalism that allows us to derive the number of GW events needed to establish a confident association between GW BBH events and AGN flares. This problem was first explored in Bartos et al. (2017a, hereafter B17), but here we consider GW events with targeted follow-up observations to catch transients, rather than an existing catalog of AGN locations. This statistical framework is presented in Section 2. In Section 3, we present results for the case of GW190521. Section 4 presents prospects for making confident associations in the future by measuring the fraction of BBH events that induce AGN flares, and Section 5 presents prospects for simultaneously using GW and AGN observations for standard siren cosmology. We conclude in Section 6.

## 2. Bayesian Framework for Associating Gravitational-wave Events with AGN Flares

In this section we describe a formalism for confidently associating GW events with AGN flares. The goal is to understand how many observations are needed to confirm the association with high confidence (Bayes factors > 100). The problem can be formulated as a signal versus background problem, where for each GW event from a BBH in an AGN disk we have  $N$  expected background flares and  $N + 1$  total expected flares.

### 2.1. $\lambda$ : The Fraction of BBH that Induce an AGN Flare

We consider a similar formalism to that described in Morgan et al. (2019) for associating IceCube neutrinos to core-collapse supernovae. In our case, we substitute the IceCube neutrinos with GW events, which may produce a signal flare if they come from an AGN, and the background supernovae with background AGN flares. We modify the formalism to be fully Bayesian, deriving a posterior probability distribution for the parameter of interest, and calculating Bayes factors.

Let  $\lambda$  be the fraction of GW events that are associated with AGN flares,  $\lambda = P(\text{AGN}|\text{GW})$ . Given a GW event  $i$  at location  $(\Omega_i^{\text{GW}}, z_i^{\text{GW}})$  and merger time  $t_i^{\text{GW}}$ , the number density of AGN flares per solid angle  $\Omega$  and per redshift  $z$  within some time

period  $t^{\text{AGN}} - t_i^{\text{GW}} < T$  is given by

$$\begin{aligned} \frac{dN_i}{d\Omega dz} \left( \Omega, z | \Omega_i^{\text{GW}}, z_i^{\text{GW}}, \lambda, T, \frac{dB}{d\Omega dz dt} \right) \\ = \lambda \delta(\Omega_i^{\text{GW}} - \Omega) \delta(z_i^{\text{GW}} - z) + T \frac{dB}{d\Omega dz dt}(\Omega, z), \end{aligned} \quad (1)$$

where  $\delta$  is the Dirac delta function. In other words, the distribution of AGN flares  $\frac{dN_i}{d\Omega dz}$  can be modeled as a mixture between an AGN flare at the same position as the GW event (expected number  $0 \leq \lambda \leq 1$ ) and the background number density of AGN flares within a time period  $T$ ,  $T \frac{dB}{d\Omega dz dt}$ . Here,  $\frac{dN_i}{d\Omega dz}$  refers to the *astrophysical* (in other words, intrinsic) distribution of AGN flares, rather than the *observed* distribution. These differ by a factor of the detection efficiency,  $P_{\text{det}}^{\text{AGN}}(\Omega, z)$ . More generally, we may consider the luminosity distribution together with the spatial density of flares in Equation (1), modeling  $dN/d\Omega dz dL$ , and  $P_{\text{det}}^{\text{AGN}}$  may depend on the apparent magnitude corresponding to  $L$  and  $z$ . Note that the luminosity of the signal AGN flare may depend on properties of the BBH, e.g., the total mass  $M_{\text{tot}}$ , in which case this can be incorporated into the model of Equation (1).

For a given GW event with data  $x_i^{\text{GW}}$ , the sky location and redshift are imperfectly measured with some joint posterior probability distribution  $p(\Omega_i^{\text{GW}}, z_i^{\text{GW}} | x_i^{\text{GW}}) \propto p(x_i^{\text{GW}} | \Omega_i^{\text{GW}}, z_i^{\text{GW}}) p(\Omega_i^{\text{GW}}, z_i^{\text{GW}})$ . Realistically, we only consider the density of AGN flares within some volume around the GW event (e.g., the 90% volume of  $p(\Omega_i^{\text{GW}}, z_i^{\text{GW}} | x_i^{\text{GW}})$ ) and accordingly normalize the background number density within this volume. We assume the location of the AGN is perfectly measured. The joint likelihood of observing the GW data  $x_i^{\text{GW}}$  and  $k$  AGN flares with positions  $\{\Omega_{ij}^{\text{AGN}}, z_{ij}^{\text{AGN}}\}_{j=1}^k$ , marginalizing over the uncertain position of the GW source  $(\Omega_i^{\text{GW}}, z_i^{\text{GW}})$ , is given by an inhomogeneous Poisson process:

$$\begin{aligned} \mathcal{L}_i &\equiv p(\{\Omega_{ij}^{\text{AGN}}, z_{ij}^{\text{AGN}}\}_{j=1}^k, x_i^{\text{GW}} | \lambda, R_B) \quad (2) \\ &= \int p(\{\Omega_{ij}^{\text{AGN}}, z_{ij}^{\text{AGN}}\}_{j=1}^k, \Omega_i^{\text{GW}}, z_i^{\text{GW}}, x_i^{\text{GW}} | \lambda, R_B) \\ &\quad \times d\Omega_i^{\text{GW}} dz_i^{\text{GW}} \quad (3) \\ &= \prod_{j=1}^k \left[ \int p(x_i^{\text{GW}} | \Omega_i^{\text{GW}}, z_i^{\text{GW}}) p_0(\Omega_i^{\text{GW}}, z_i^{\text{GW}}) \right. \\ &\quad \left. \times \frac{dN_i}{d\Omega dz}(\Omega_j, z_j | \Omega_i^{\text{GW}}, z_i^{\text{GW}}, \lambda, R_B) d\Omega_i^{\text{GW}} dz_i^{\text{GW}} \right] e^{-\mu_i}, \quad (5) \end{aligned}$$

where  $p_0(z, \Omega)$  refers to the prior on the redshift and sky position of the GW source, we define the background rate  $R_B = T \frac{dB}{d\Omega dz dt}$  for simplicity of notation, and  $\mu_i$  is defined below. The background term does not carry the GW term because it does not depend on the GW position and distance, so that the GW part integrates to 1 in the marginalization over  $\Omega_i^{\text{GW}}, z_i^{\text{GW}}$ . In the above,  $\mu_i$  refers to the expected number of *observed* AGN flares:

$$\mu_i \equiv \int \frac{dN_i}{d\Omega dz} P_{\text{det}}^{\text{AGN}}(\Omega, z) d\Omega dz. \quad (6)$$

The background term in  $\frac{dN_i}{d\Omega dz}$  does not depend on  $\lambda$ , so if we are interested in the posterior over  $\lambda$ , we can consider only the first

term in the right-hand side of Equation (1) when computing  $\mu_i$ . Finally, the likelihood becomes

$$\mathcal{L}_i \propto \prod_{j=1}^k [\lambda p(x_i^{\text{GW}} | \Omega_{ij}^{\text{AGN}}, z_{ij}^{\text{AGN}}) p_0(\Omega_{ij}^{\text{AGN}}, z_{ij}^{\text{AGN}}) + R_B(\Omega_{ij}^{\text{AGN}}, z_{ij}^{\text{AGN}})] e^{-\mu_i}. \quad (7)$$

In this work, we assume that the prior  $p_0$  scales as  $\propto d_L^2$ , where  $d_L$  is the luminosity distance, and it is uniform in sky position  $\Omega$ . This is a rather common assumption for GW events, consistent with BBH events scaling with the volume. In the cases where no AGN flare is detected in a follow-up (at a location at which the GW localization likelihood has nonzero support), the likelihood of that specific follow-up reduces to

$$\mathcal{L}_i \propto e^{-\mu_i}, \quad (8)$$

which tends to prefer lower values of  $\lambda$ , and it is therefore also informative to perform a follow-up that does not detect any flares. Note that the fraction of GW events with associated AGN flares,  $\lambda$ , and the number density of background AGN flares,  $\frac{dB}{d\Omega dz dt}$ , are common to all GW events  $i$ . For example, we can measure the posterior probability on  $\lambda$  by combining observations from  $N$  GW events:

$$p\left(\lambda | \{x_i^{\text{GW}}\}_{i=1}^N, \{\{\Omega_{ij}^{\text{AGN}}, z_{ij}^{\text{AGN}}\}_{j=1}^k\}_{i=1}^N, T, \frac{dB}{d\Omega dz dt}\right) \propto p(\lambda) \prod_{i=1}^N \mathcal{L}_i, \quad (9)$$

where  $p(\lambda)$  is the prior on  $\lambda$ , which is assumed to be uniform between 0 and 1 throughout this Letter, given our lack of knowledge of its value. With enough GW events, we will be able to measure  $\lambda$  and confidently determine whether  $\lambda > 0$ ; in other words, whether a nonzero fraction of GW events are associated with AGN flares. We refer the reader to Berman (1986) and Baddeley et al. (2015) for previous works and existing tools applying inhomogeneous Poisson models to 2D spatial point processes.

For a specific GW event  $i$  with AGN counterpart  $ij$ , the probability  $p_{ij}^{\text{GW-AGN}}$  that the AGN flare is associated with the GW event is given by

$$p_{ij}^{\text{GW-AGN}} = \frac{\lambda p(\Omega_{ij}^{\text{AGN}}, z_{ij}^{\text{AGN}} | d_i^{\text{GW}})}{\lambda p(\Omega_{ij}^{\text{AGN}}, z_{ij}^{\text{AGN}} | d_i^{\text{GW}}) + T \frac{dB}{d\Omega dz dt}(\Omega_{ij}^{\text{AGN}}, z_{ij}^{\text{AGN}})}. \quad (10)$$

This can be inferred jointly with  $\lambda$ .

In the above, when writing  $p(\Omega, z | x^{\text{GW}})$ , we have assumed perfect knowledge of the cosmological parameters  $\vec{\theta} \equiv (H_0, \Omega_m, \dots)$ . The GW data yield a measurement of the luminosity distance  $d_L$ , related to  $z$  via  $\vec{\theta}$ . If we assume a prior distribution  $p(\vec{\theta})$ , we must marginalize out this prior:

$$p(\Omega, z | x^{\text{GW}}) = \int p(\Omega, z | x^{\text{GW}}, \vec{\theta}) p(\vec{\theta}) d\vec{\theta} \quad (11)$$

$$= \int p(\Omega, d_L(z, \vec{\theta}) | x^{\text{GW}}) p(\vec{\theta}) d\vec{\theta}. \quad (12)$$

Because an uncertain cosmology implies a larger localization volume for a given GW event, we must ensure that the background rate density is normalized over this larger volume as well, especially if we are using the results to infer cosmological

parameters. This will tend to increase the expected number of background AGN flares.

## 2.2. Standard Sirens

For GW events with a counterpart, a unique host galaxy, and therefore a cosmological redshift, can be identified. Events without a counterpart require a marginalization over all potential host galaxies and therefore provide a less precise estimate of cosmological parameters (e.g., Chen et al. 2018). In the case of AGN flares, given the possible contamination of background events, the cosmological parameter estimation problem becomes intermediate between the dark-siren and unique-counterpart cases.

Let us consider  $N$  GW events  $\{x_i^{\text{GW}}\}_{i=1}^N$ , which have been followed up with observations of the AGN in the relevant volumes. Considering the follow-up data  $\{x_i^{\text{AGN}}\}_{i=1}^N \equiv \{\{\Omega_{ij}^{\text{AGN}}, z_{ij}^{\text{AGN}}\}_{j=1}^k\}_{i=1}^N$ , the posterior on the cosmological parameters  $\vec{\theta}$  is

$$p(\vec{\theta} | \{x_i^{\text{AGN}}\}_{i=1}^N, \{x_i^{\text{GW}}\}_{i=1}^N) \propto p(\vec{\theta}) \int d\lambda p(\lambda) \prod_i^N \mathcal{L}_i(\vec{\theta}, \lambda). \quad (13)$$

Going back to Equation (2) and modifying the likelihood to be conditioned on the cosmology, we get

$$\mathcal{L}_i(\vec{\theta}, \lambda) \propto \prod_{j=1}^k [\lambda p(x_i^{\text{GW}} | \Omega_{ij}^{\text{AGN}}, d_L(z_{ij}^{\text{AGN}}, \vec{\theta})) p_0(\Omega_{ij}^{\text{AGN}}, z_{ij}^{\text{AGN}}) + R_B(\Omega_{ij}^{\text{AGN}}, z_{ij}^{\text{AGN}}, \vec{\theta})] e^{-\mu_i}. \quad (14)$$

If no flares are identified in a follow-up, the likelihood is that of Equation (8). If there is no GW follow-up, the AGN likelihood is uninformative. However, we note that one can substitute the GW prior  $p_0(\Omega, z)$  for a galaxy catalog (or, equivalently, replace  $p_0$  with a galaxy catalog posterior  $p(\Omega, z | x_{\text{gal}})$ ). In this case, the likelihood will reduce to that of the statistical standard siren method (Del Pozzo 2012; Fishbach et al. 2018; Palmese et al. 2020).

Here we have ignored GW selection effects, which play an important role especially for cosmological measurements. To account for GW selection effects, Equation (14) must be divided by a term  $\beta(\vec{\theta})$ , so that it integrates to unity over detectable GW data sets (e.g., Mandel et al. 2018).

## 3. The Case of GW190521

The AGN J124942.3+344929 is not particularly well placed in the LIGO/Virgo GW190521 sky localization map. Nonetheless, the position on the sky has support in line-of-sight probability. We wish to estimate a probability of chance occurrence.

As the AGN luminosity function is known over the range of redshifts of interest from, e.g., Hopkins et al. (2007) and Shen et al. (2020), our program is straightforward. For a given search limiting magnitude, integrate down the luminosity function to the luminosity corresponding to that magnitude limit of  $z$ , then multiply by the spatial volume of the search area. This yields the average number of quasars in the volume. The statistics of quasar variability may then be assessed to estimate the number of quasars varying over the timescale of interest and the magnitude difference required to be labeled a flare. Simply, the expected number of flares is  $N_f = \text{Vol} \cdot \phi \cdot f_f$ , where  $\phi$  is the



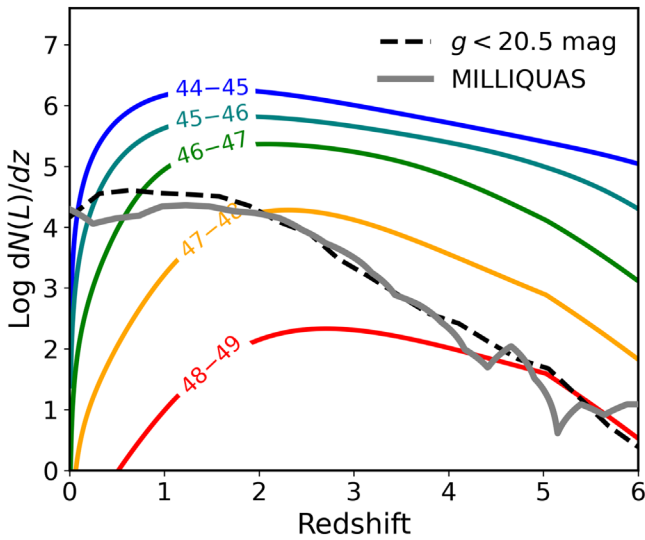


**Figure 1.** Redshift distribution of the number of AGNs using the quasar luminosity function from Hopkins et al. (2007) in an area of the sky corresponding to the 90% CI GW190521 sky map. The thick solid lines are the redshift distributions in various luminosity intervals (in  $\text{Log}(L_{\text{bol}}/[\text{erg s}^{-1}])$ ). The dashed black line is the redshift distribution with a flux limit of  $g < 20.5$  AB mag. The gray line is the redshift distribution of AGNs from the MILLIQUAS Catalog that lie within the 90% CI GW sky map. It is clear that there order of  $\sim 10^4$  AGNs around the redshift  $z = 0.64_{-0.28}^{+0.28}$  of the event.

volume density of quasars and  $f_f$  is the fraction of those that vary enough to be labeled a flare.

GW190521 has a spectacularly large localization volume, due to the large 90% sky localization of  $936 \text{ deg}^2$  and the large mean luminosity distance of  $3.92_{-1.95}^{+2.19} \text{ Gpc}$  (Abbott et al. 2020a). We calculate the spatial volume of localization of GW190521 using the the sky map from Abbott et al. (2020a) and the software from Singer & Price (2016) and Singer et al. (2016a, 2016b). We find that the 90% credible interval (CI) comoving volume is  $4.1 \text{ Gpc}^3$ , and the 99% volume is  $9.1 \text{ Gpc}^3$ . For context, see the other localization volumes in Table 1. For our  $N_f$  calculation we take  $\text{Vol} = 4.1 \text{ Gpc}^3$ .

To estimate the number of AGNs in the localization volume, we use the quasar luminosity function (QLF) from Hopkins et al. (2007), given in a dual power-law form:

$$\phi(L) = \frac{\phi_*}{(L/L_*)^{\gamma_1} + (L/L_*)^{\gamma_2}},$$

where at  $z = 1$  the parameters of the fit are  $\log \phi_* = -4.6$  quasars  $\text{Mpc}^{-1} / \log(L)$ ,  $\log(L_*/L_\odot) = 12.6$ ,  $\gamma_1 = -0.4$ ,  $\gamma_2 = -2.2$ , and where  $L$  is the bolometric luminosity. The parameter values vary as a function of  $z$  as the quasar population evolves. Note the faint quasar power law is shallow while the luminous quasar power law is steep. In Figure 1 we show the  $dN(L)/dz$  in the 90% sky area, assuming a concordance cosmology for the volume. The numbers are dominated by quasars at or below the break in the dual power law. How far down the LF one sees at a given  $z$  is an observational question. For the ZTF limiting magnitude of  $g < 20.5$  AB mag, we integrate down the LF to the corresponding limiting luminosity, assuming  $L_{\text{bol}} = 10 L_{\text{band}}$ , where  $L_{\text{band}}$  is the luminosity in an optical band following Hopkins et al. (2007). The result is the black dashed line in

Figure 1, which shows the  $dN/dz$  of quasars in the area. We find that there are  $\sim 34,000$  AGNs in the 90% localization area out to  $z < 1$ . For comparison, we show the redshift distribution of quasars in the Million Quasars (MILLIQUAS) Catalog (Flesch 2019) in the 90% localization area. The dominant source of AGNs in MILLIQUAS are Sloan Digital Sky Survey (SDSS) quasars. While we have computed the number of AGNs using the luminosity function, its redshift evolution, and an apparent magnitude limit, our numbers are equivalent to considering a uniform AGN number density of  $n_{\text{AGN}} = 10^{-5} \text{ Mpc}^{-3}$  (which is lower than the fiducial value of  $z \approx 0.2$  type-I AGNs considered in B17,  $n_{\text{AGN}} = 10^{-4.75} \text{ Mpc}^{-3}$ ), since that would translate into a total number of AGN in the 90% volume  $\text{Vol} = 4 \times 10^9 \text{ Mpc}^3$  of 40,000.

We use the prescription of Hopkins et al. (2007) to calculate the fraction of type-I quasars, now known as optically unobscured AGNs. Originally the difference between type-I and type-II AGNs was whether they showed broad+narrow lines (type-I) or only narrow lines in the optical spectrum. This is important when computing the probability of chance coincidence for optical flares, because a flare in the accretion disk is expected to be obscured from view, at least in the optical. It does not necessarily mean that a BBH merger could not happen in an obscured AGN, or that a flare could not be observed as a “reprocessed” flare at other, perhaps longer, wavelengths (see Kool et al. 2020 for an example of transient candidate in an obscured AGN). Similarly, one may want to exclude blazars from the AGN sample as a flare in a blazar would not be easily identified due to their extreme variability. However, the fraction of blazars in an AGN sample is of the subpercent level (e.g. Urry & Padovani 1995), so their inclusion does not significantly affect our estimates. We find that there are  $\sim 7400$  type-I AGNs in the  $936 \text{ deg}^2$  down to  $g < 20.5$ . For our  $N_f$  calculation we take  $\text{Vol} \cdot \phi = 7400$  AGNs. This is different from the  $\sim 3000$  AGNs considered in G20 for two main reasons. First, they consider the volume covered by ZTF, which is roughly half of the total volume in the preliminary sky map (LIGO Scientific Collaboration & Virgo Collaboration 2019). Second, we use the updated sky map from LIGO/Virgo, which encompasses a larger volume than the preliminary LALInference map used in G20 (4 versus  $2 \text{ Gpc}^3$ ). Alternatively, if one wants to take into account AGNs below the  $g < 20.5$  limit, and consider all type-I AGNs down to our bolometric luminosity limit of  $10^{44} \text{ erg s}^{-1}$ , the number density is  $\sim 10^{-4.5} \text{ Mpc}^{-3}$ , which results in a number of AGNs in the 4 Gpc volume of  $\text{Vol} \cdot \phi \sim 130,000$ .

The labeling of a quasar variability event a flare is a judgment. Most or all quasars vary; searching for point sources that vary is one of the very best ways to find quasars. A common model for quasar variability is the damped random walk (DRW), yet this is a particular model and questions about its general applicability remain in the literature—see, e.g., Kasliwal et al. (2015) for the question of short timescales, and Kozłowski (2016) for a measurement of the distribution of quasar variability power-law indices about and biased from the DRW index. Graham et al. (2020) use a DRW model to estimate the probability of chance occurrence, and the literature suggests treating this with caution. We will instead use structure functions (SFs), which are a more general description of variability; see Kozłowski (2016) for a review. The structure

function is

$$\text{SF}(\Delta t) = \text{SF}_0 \left( \frac{\Delta t}{\Delta t_0} \right)^\gamma, \quad (15)$$

where SF is measured in magnitudes ( $\Delta m$ ),  $\text{SF}_0$  is the  $\Delta m$  measured at some time  $\Delta t_0$ , say 100 days, and  $\gamma$  is the power-law index. The SF is not a physical model, but an observational, statistical description of AGN variability. The DRW is a special case of the SF:

$$\text{SF}(\Delta t) = \text{SF}_\infty (1 - e^{-\Delta t/\tau})^{0.5}, \quad (16)$$

where  $\text{SF}_\infty$  is measured as some time suitably long compared to the problem. The timescale  $\tau$  may be the timescale of a model related, for example, to black hole mass. Of note is that for the DRW the power-law index is fixed at 0.5; the SF measures this as its  $\gamma$  parameter.

Graham et al. (2020) report AGN J124942.3 + 344929 varied by  $\approx 0.4$  mag over 50 days. We estimate the probability of this using SF measurements from Kimura et al. (2020), who present HSC optical data for a robust sample of AGNs down to  $r \lesssim 23.5$ , excluding blazars. Their Figure 18 shows the SF versus  $\Delta t$ . For  $g$  band and  $\Delta t_0 \sim 30$  days, they find  $\text{SF} \approx 0.128$ . We will use  $\Delta m = 0.4$  mag. One interprets the SF as the timescale-dependent standard deviation  $\sigma$  of a normal distribution centered on 0, which describes the probability distribution of having a  $\Delta m$  change in magnitude for an AGN, and one calculates the one-sided probability corresponding to  $\Delta m > 0.4$  (because this is one-sided, we are only considering changes in magnitude toward brighter values),  $f_f \sim 10^{-4}$ . By comparison, Graham et al. (2020) estimated that the chance of their flare model fitting any ZTF AGN lightcurve is  $\sim 5 \times 10^{-6}$ , assuming a DRW model. The difference between the flare probability of Graham et al. (2020) and ours is the fact that they required a fit with a specific flare shape, following the model of Graham et al. (2017), to the available sample of AGNs, while we only require a magnitude change over a timescale. The magnitude change requirement does not imply that we are considering step-like functions or rise-only lightcurves as flares in this analysis, as those shapes are not typical of AGN lightcurves (see, e.g., Smith et al. 2018). Our requirement does however imply that we are selecting a larger sample of flares than that of G20, hence the larger flare probability.

We are now ready to compute  $N_f = \text{Vol} \cdot \phi \cdot f_f$ . Our estimate is  $N_f = 7400 \times 10^{-4} \sim 0.74$  flares in the area. This translates to a 70% probability of chance coincidence of an AGN flare of  $\Delta m > 0.4$  in the 90% GW localization. Even using the Graham et al. (2020) estimate that the chance of their flare model fitting any ZTF AGN lightcurve is  $\sim 5 \times 10^{-6}$  using our calculated unobscured AGN numbers, this implies a  $\sim 4\%$  probability of chance coincidence. To further understand if the flare probability we find is reasonable for this specific AGN, and for comparison with G20, we use the long-term available data to fit a DRW model. We fit the SF to the unbinned CRTS (Djorgovski et al. 2011) and ZTF (Masci et al. 2018; Bellm et al. 2018) data following the method of Kelly et al. (2009) using the CELERITE code (Foreman-Mackey et al. 2017). The uncertainties in the CRTS photometry are rescaled using the prescription of Graham et al. (2017), while the offset used to combine CRTS with ZTF is from Graham et al. (2020). We mask out the lightcurve portion associated with the flare in 2019, and find that the parameters of Equation (16) are  $\ln(\text{SF}_\infty/\text{mag}) = -0.74_{-0.11}^{+0.18}$  and  $\ln(\tau/\text{days}) = 6.04_{-0.59}^{+0.94}$  in the

observed frame. For a timescale of 40 days (observed frame), the maximum likelihood values of the DRW correspond to an SF of  $\sim 0.14$ ; thus the probability of observing a flare of magnitude 0.4 in this AGN is  $\sim 10^{-3}$ . We note that the SF estimate from the DRW fit is consistent within  $1\sigma$  with the HSC SF we use, and conclude that the observed flare could be associated with stochastic AGN variability, and that our  $f_f$  calculation for a generic AGN is reasonable also for the AGN in question.

Clearly how one does the  $f_f$  calculation matters, but we argue that probabilities of 4% to 70% of a chance occurrence suggests that the flare in AGN J124942.3 + 344929 is consistent with being a background flare. It is worth recalling that ZTF did not cover the 90% spatial localization, as their observations covered  $\approx 50\%$  of the probability in sky localization. In the future, it will be preferable to constrain the flare probability for AGNs empirically using the flare model expected for this BBH channel, rather than using models, such as the SF or DRW, that assume Gaussian processes.

An important note is that our simple calculation is conservative, in the sense that a larger number of AGNs could be considered. We did not include low-luminosity AGNs (LLAGN)  $L_{\text{bol}} < 10^{44} \text{ erg s}^{-1}$ , which are more abundant than quasars in particular at low redshift (e.g., Hao et al. 2005), although McKernan et al. (2018) and Ford & McKernan (2019) show that LLAGN cannot be very efficient sites for BBH mergers, or the LIGO/Virgo volumetric BBH rate should be larger than what measured. In addition, we have considered a minimum  $\Delta m = 0.4$ , while a lower cut, say at 0.3, would result in an order of magnitude more probable flares, and therefore an order of magnitude more expected flares, bringing the probability of chance occurrence in the GW region to 40%–100%.

An extension to our analysis is to use the spatial distribution of GW distance and distance uncertainty in the calculation of the limiting luminosity of the AGNs observed from the AGN luminosity function, and to do so over the (much larger) 99% confidence level localization. We do not expect this to significantly affect the result, and the high probability of chance coincidence does not provide sufficient motivation to pursue it. However, it is worth pursuing the question of how to constrain the possibility that AGN accretion disks do provide the site of BBH mergers.

#### 4. Constraining the Fraction of BBH Inducing an AGN Flare

The question of which formation channel(s) are responsible for creating BBH systems is hotly debated. It is of considerable interest to evaluate the fraction of BBH events that come from AGN disks. In this section we show the results of applying the Bayesian method described in Section 2 to simulations of future GW events in pursuit of the number of events necessary to constrain the fraction  $\lambda$  of BBH events that produce AGN flares.

First, we assume GW events like GW190521. In this case, we draw the distances and sky positions of the signal events from the sky map posterior samples of GW190521. This is equivalent to assuming different realizations of the same event, and it is useful to understand how many events are needed to reach a confident association if only events having a probability of chance coincidence comparable to that of GW190521 are considered. The background events are drawn from a Poisson distribution with an expectation value of  $4 \times 10^9 \times 10^{-4} \times 10^{-4.5}$  following the number of flares from the HSC  $g$ -band SF and the number of

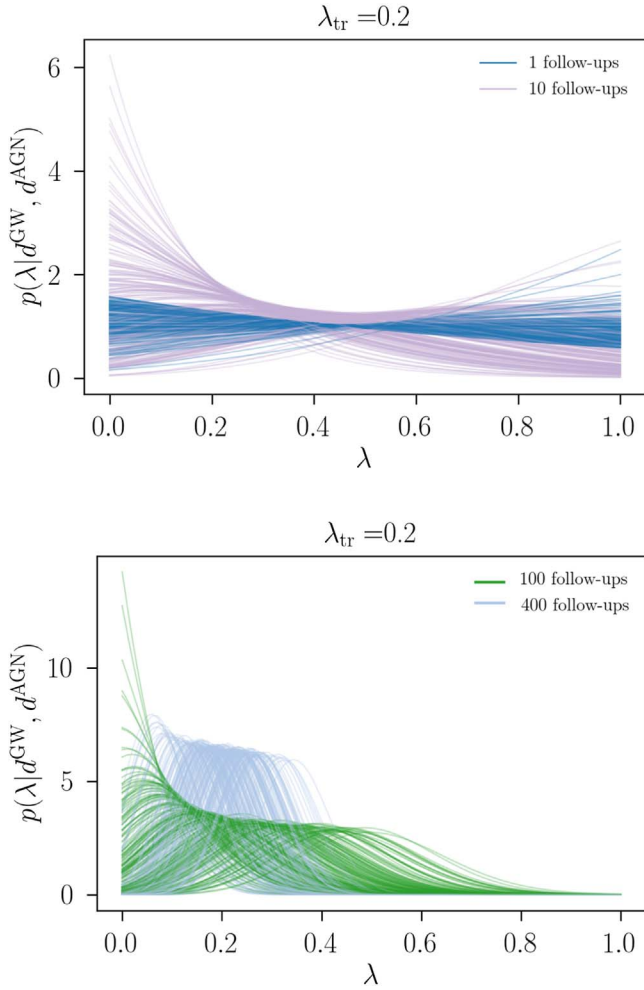


**Figure 2.** Posteriors for  $\lambda$  from 200 sets of simulations of 400 follow-up observations of GW190521-like events for an input value of  $\lambda = 0.2$ , as an example of the method. The posteriors are derived for four values of number of follow-ups, and for a uniform prior in  $\lambda$  between 0 and 1. It is clear that the posterior becomes more constraining around the true value of  $\lambda$  as the number of follow-up observations increases.

AGNs in the 90% volume. The choice of the number of AGNs that would contribute to the background flares depends on a number of factors, including the depth of the survey, the wavelengths observed, and the redshift of the event. We therefore decide in the following to make the most conservative assumption, and assume that the average number density of those AGNs is  $10^{-4.5} \text{ Mpc}^{-3}$ , which would include all type-I AGNs down to  $L_{\text{bol}} = 10^{44} \text{ erg s}^{-1}$ . We generate 200 sets of simulations of up to 800 follow-ups for different input values of  $\lambda$  between 0 and 1. As an example, the  $\lambda$  posteriors for a truth value of  $\lambda_{\text{tr}} = 0.2$ , for four values of number of follow-ups, and for a uniform prior in  $\lambda$  between 0 and 1 are shown in Figure 2. It is clear that the posterior becomes more constrained around the true value of  $\lambda$  as the number of follow-ups increases.

We repeat the same procedure using better-localized sky maps, namely, those of GW190701\_203306 (Abbott et al. 2020a; 99% CI comoving volume  $0.087 \text{ Gpc}^3$ ), GW170814 (Abbott et al. 2017b; 99% CI volume  $1.5 \times 10^{-4} \text{ Gpc}^3$ ), and GW190814 (Abbott et al. 2020c; 99% CI volume  $9.2 \times 10^{-5} \text{ Gpc}^3$ ). We scale the expected number of background events based on each event’s volume. We then compute the Bayes factor  $K$  for a model with  $\lambda > 0$  (which is taken to be the mode  $\bar{\lambda}$  of the  $\lambda$  posterior)

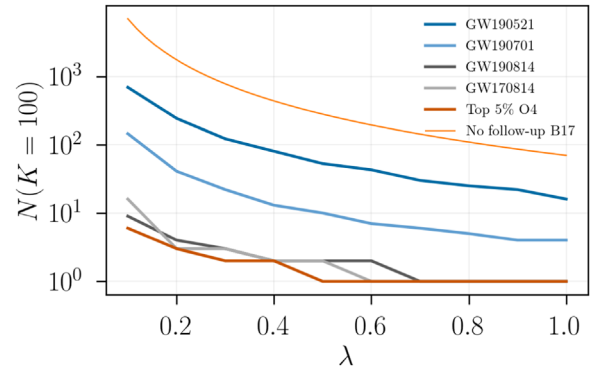


**Figure 3.** Number of GW events to be followed up to obtain a confident association (i.e., for a Bayes factor  $K = 100$ ) between AGN flares and BBH events, as a function of the true input value of  $\lambda$  in the simulations. Each curve corresponds to a different fixed GW sky map, with a range of localization volumes (from  $\sim 10^{-4}$  to  $10 \text{ Gpc}^3$  at 99% CI). This figure applies to the ideal case in which the AGN flares associated with the GW events are all detectable (we assume a magnitude limit  $g < 20.5$ ). The orange line shows a comparison with the result from Bartos et al. (2017a, hereafter B17), who do not consider follow-up observations of AGN flares, but instead compare the GW localizations with AGN positions. The other differences with B17 are that their  $N$  corresponds to the number of events needed to reach  $3\sigma$  using a  $p$ -value statistical method, and that they consider a slightly lower AGN number density.

versus a model with  $\lambda = 0$  using the likelihoods obtained from our simulations, as the Savage-Dickey density ratio:

$$K = \frac{p(x|\lambda = \bar{\lambda})}{p(x|\lambda = 0)}, \quad (17)$$

where  $x$  is the GW and AGN data. We consider the AGN association (i.e.,  $\lambda > 0$ , because at least a fraction of the BBH come from AGNs) to be confident if  $K > 100$ . The number of follow-up observations needed to reach this requirement as a function of the true value of  $\lambda$  given in input is shown in Figure 3 for different sky maps. It is clear that for poorly localized events like GW190521, tens of GW follow-up campaigns are required in order to make a confident association, even in the most optimistic case where  $\lambda_{\text{tr}} = 1$  and we can detect all AGNs where the BBH merger could happen. Only a few to tens of events are needed to make a confident association for better-localized events such as GW170814 or GW190814 down to  $\lambda_{\text{tr}} = 0.1$ . This is an obvious consequence of the fact that the number of background contaminants scales with the comoving volume, and that the localization volume of these events is orders of magnitude lower than the one of GW190521.

We compare our results with the predictions by B17 who use only GW localizations (i.e., without follow-up observations) to probe the origin of BBH mergers and to potentially associate them with AGNs. Figure 3 shows that we find a similar scaling relation of the number of events required to reach  $K = 100$  as a function of  $\lambda$  like theirs, although slightly less steep than  $N(K = 100) \propto \lambda^{-2}$ . The main differences with the B17 predictions, other than follow-up observations, are that their  $N$  corresponds to the number of events needed to reach  $3\sigma$  using a  $p$ -value statistical method (so that here the scaling of the number of events needed could be different as we are not directly considering the width of a distribution), and that they consider a fixed (in redshift) and lower AGN number density.

Next, we consider the expected constraints that can be derived from the upcoming LIGO/Virgo/KAGRA observing run O4, expected to start in 2022. We consider the AGN flare



observable  $\Delta m$ , the change in the AGN magnitude over time, as above, and use it to compute the expected number of background events using the same SF. We assume that for BBH mergers in AGN disks, the observed  $\Delta m$  depends on the total source-frame BBH mass according to the prescription in McKernan et al. (2019), also used in Graham et al. (2020), where the counterpart brightness is proportional to  $M_{\text{BBH}}^2$ . The observed flare for a generic BBH in an AGN disk, expressed in terms of the total mass  $M_{\text{BBH},19}$ , the potential counterpart flux  $F_c$ , and AGN flux  $F_{\text{AGN}}$  for GW190521 will have

$$\Delta m = -2.5 \log \left[ 1 + \frac{M_{\text{BBH}}^2}{M_{\text{BBH},19}^2} \left( \frac{F_c}{F_{\text{AGN}}} \right)_{\text{GW190521}} \right]. \quad (18)$$

Ideally, one would rescale the AGN flux as well based on the AGN luminosity function for each potential host AGN in the simulations. However, using the flux of SDSS J124942.3+344929 as a “fiducial” AGN flux is reasonable because its bolometric luminosity is  $\log(L/L_\odot) \approx 12.3$ , and therefore very close to the  $L_*$  value from Hopkins et al. (2007) at  $z = 0.5$ , where  $\log(L_*/L_\odot) = 12.24$ . This implies that AGNs brighter than SDSS J124942.3+344929 are rare, while the majority of AGN we consider here will be less bright, and therefore a counterpart of the same luminosity would be even more easily detected.

We simulate GW events using the BAYESTAR software (Singer & Price 2016; Singer et al. 2016a, 2016b), also based on tools from LALSuite (LIGO Scientific Collaboration 2018). We assume sensitivity curves for Advanced LIGO and Virgo at O4 sensitivity as published in Abbott et al. (2018).<sup>7</sup> We also consider the addition of KAGRA during O4 with the sensitivity curve from <https://dcc.ligo.org/LIGO-T2000012/public>, having a BNS range of  $\sim 80$  Mpc. The simulation includes 10,000 BBHs following a distribution that is uniform in comoving volume, assuming a Planck Collaboration et al. (2018) cosmology. We assume IMRPhenomD waveforms both for the injections and reconstructions. We modify the BAYESTAR code so that the primary BHs follow a mass function based on the best fit from the “power-law + peak” model of Abbott et al. (2020d). The primary mass distribution is described by a power law with index 1.6, plus a Gaussian peak centered on  $33 M_\odot$  and with standard deviation of  $6 M_\odot$ . The events following the power law comprise 90% of the sample, while the events from the Gaussian peak are 10%. The maximum BH mass considered is  $100 M_\odot$ , and the BHs follow a uniform spin distribution between  $(-1, 1)$ . After the 10,000 injections are made, we run a matched-filter search to retrieve the detected events. A detection is made when at least two detectors reach a single-detector signal-to-noise ratio (S/N)  $> 4$  and the network S/N is  $> 12$ . Gaussian noise is added to the measured S/N. In the last step, we reconstruct BAYESTAR sky maps for the detection. The reconstruction is made assuming a GW prior  $p_0$  which scales as  $\propto d_L^2$ , where  $d_L$  is the luminosity distance, and it is uniform in sky position  $\Omega$ .

We select BBHs with  $M_{\text{tot}} > 50 M_\odot$ , because they are assumed to give rise to brighter flares than lower-mass events. Out of 2401 simulated detections, 1131 events meet the mass cut. For each event, we calculate the expected number of background events based on the 90% CI volume from the BAYESTAR reconstruction and the SF at the expected flare

magnitude given the mass of the binary, assuming a conservative number density of AGNs of  $10^{-4.5} \text{ Mpc}^{-3}$ . The final number we use to define the events of interest is the number of expected background events, which is ultimately what defines how quickly one can reach a confident association.

Using the population fits from Abbott et al. (2020d), we infer that the astrophysical merger rate for BBH systems with  $M_{\text{tot}} > 50 M_\odot$  is  $3\text{--}6 \text{ Gpc}^{-3} \text{ yr}^{-1}$  (90% credible interval). At the sensitivity expected for O4, our simulations predict 59–117 detections in this mass range per year of observation. We find that  $\sim 4\text{--}6$  events per year ( $\sim 5\%$  of all  $M_{\text{tot}} > 50 M_\odot$  BBH detections) will be better (i.e., they will have a smaller number of expected background flares) than the forecasts above labeled as GW170814, 7–10 per year ( $\sim 8\%$ ) will be better than the forecasts labeled as GW190701, and  $\sim 19\text{--}28$  ( $\sim 24\%$ ) will be better than GW190521. It is clear from Figure 3 that the top 5% events in the mass range of interest are those that will provide the most significant constraints: following up these well-localized and brighter events will allow us to confidently say if  $\lambda > 0$ , at least in the case where the true value of lambda is  $\lambda_{\text{tr}} \gtrsim 0.1\text{--}0.2$  (3–6 events required) for a year-long O4 run. On the other hand, it is clear from Figure 3 that if no follow-up observations are obtained, the GW–AGN association is likely to only be possible if  $\lambda \gtrsim 0.4$  during a one-year-long O4 run, since  $> 500$  events are needed for  $\lambda < 0.4$ , at least in this fiducial case. The motivation for pushing down to lower  $\lambda$  values is that current detections suggest that there are multiple BBH formation channels at play (Abbott et al. 2020d; Wong et al. 2020; Zevin et al. 2020; Bouffanais et al. 2021), and that one single channel does not contribute to more than  $\sim 70\%$  of all the BBHs (Zevin et al. 2020), i.e., it is likely that  $\lambda_{\text{tr}} < 0.7$ .

We note that the method for choosing the top 3% events for this forecast does not solely rely on the localization volume, but also on the total mass of the binary. We therefore suggest that an estimate of the BBH total mass could be an interesting parameter to share with the astronomical community during the next LIGO/Virgo/KAGRA observing runs.

In the top panel of Figure 4 we show the scaling of the uncertainty on  $\lambda$  from the simulation as a function of the number of events followed up, for different events. As expected, better-localized events have a smaller number of background flares, and reach a better precision with a smaller number of follow-ups than events like GW190521. The effect of varying the number of background flares can be better seen in the bottom panel of Figure 4, where the map is GW190521 for all lines and the input value of  $\lambda$  is fixed to 0.1, while the density of an AGN (each considered with its own probability of flaring) is changed between  $10^{-7}$  and  $10^{-4} \text{ Mpc}^{-3}$ . The scaling roughly follows  $\propto 1/\sqrt{N}$ , where  $N$  is the number of follow-up observations considered.

It should be noted that the results above are valid when considering bright flares with a probability computed from structure functions (or any other flare happening with a probability of  $\sim 10^{-4}$  in an AGN at any given time), and for AGNs brighter than  $L_{\text{bol}} = 10^{44} \text{ erg s}^{-1}$ . We are not aware of a theoretical argument that would set a specific threshold for the flare magnitude, so we have showed most of our results based on the follow-up details of GW190521 and this luminosity limit. As more sophisticated theoretical modeling of the BBH merger mechanism in AGNs becomes available, it will be possible to rescale our results based on new thresholds.

<sup>7</sup> <https://dcc.ligo.org/LIGO-T2000012/public>

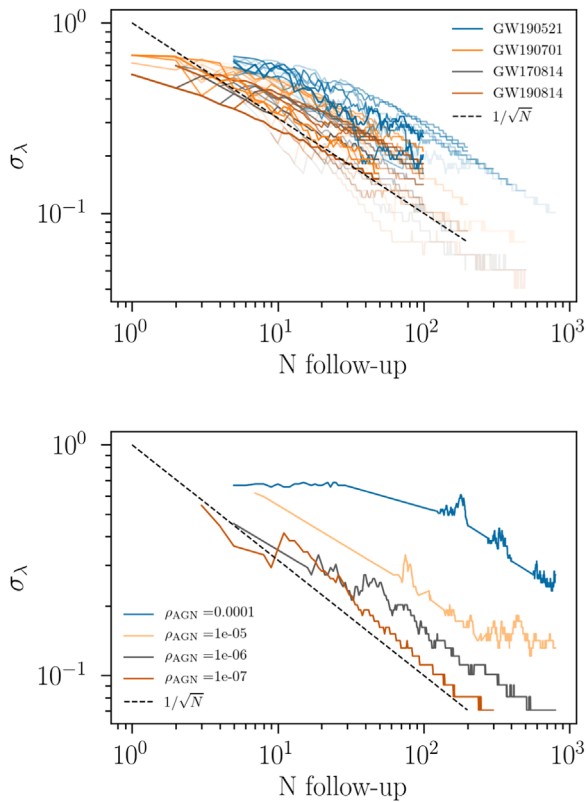


**Figure 4.** Top: expected uncertainty (68% CI) on the fraction  $\lambda$  of GW BBHs that can be associated with AGN flares, as a function of the number of follow-up observations performed, for sky maps of different GW events. The transparency of the lines is given by the input parameter of  $\lambda$  assumed in the simulations, between 0.1 (lighter lines) to 1 (heavier lines). A  $1/\sqrt{N}$  scaling is shown for reference. Simulations using higher  $\lambda$  values or smaller localization volumes end earlier since they need fewer events to reach the required precision. Bottom: same as the top panel, except the sky map is fixed to that of GW190521,  $\lambda$  is fixed to 0.1, and the number density of AGNs is changed.

## 5. Cosmological Parameter Estimation in a Noisy Source Identification Environment

Using a contaminated sample of AGN flares as GW counterparts, without accounting for chance coincidences, will recover biased cosmological parameters. For  $H_0$  measurements, the bias depends both on the value of  $\lambda$  (lower values of  $\lambda$  will result in higher contamination of background flares), and on the detection threshold of AGN flares. If we assume that we can see all AGN flares, then most background flares live at larger distances, giving rise to most likely measurements of  $H_0$  that are larger than the true value of the Hubble constant. In reality, it is likely that we will be more sensitive to the lower-redshift flares from magnitude-limited sky surveys, and this would tend to bias  $H_0$  low rather than high. For well-localized events (similar to GW170814, for example), the rate of background flares is sufficiently low that the probability of chance coincidence is lowered and there is less risk of biasing cosmological measurements. In general, however, the contribution from background flares must be properly accounted for.

The framework presented in Section 2 is able to provide unbiased constraints on  $\lambda$  and cosmological parameters. For this example, we fix the cosmology to a flat  $\Lambda$ CDM scenario with  $\Omega_m = 0.3$ , and only let  $H_0$  vary. We simulate signal and background flares assuming  $H_0 = 70 \text{ km s}^{-1} \text{ Mpc}^{-1}$ , and we randomly draw 10 events from the top 5% of the simulated events for LIGO/Virgo/KAGRA O4 with total rest-frame

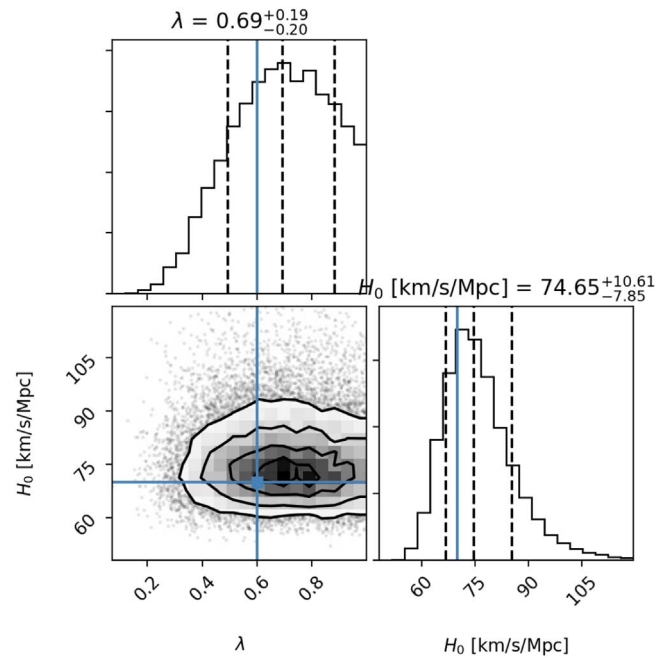


**Figure 5.** Joint posterior of the Hubble constant and the fraction  $\lambda$  of BBHs giving rise to flares in AGNs from 10 BBHs drawn from the top 5% of the simulated events for LIGO/Virgo/KAGRA O4 with a total rest-frame mass  $>50 M_\odot$ . The top events are chosen based on the expected number of background flares, which in turn depends on the localization volume and the flare magnitude (which scales with the total rest-frame BBH mass). The blue square shows the input values of the Hubble constant and of  $\lambda$  for the simulation. This figure shows that our statistical framework is able to recover the true values of these parameters, and that the follow-up of 10 well-localized GW BBHs can bring a  $\sim 12\%$  measurement of  $H_0$ , provided that  $\lambda \sim 0.6$ .

mass  $>50 M_\odot$ , following the simulations described in Section 4. We assume that 60% of the events give rise to an AGN flare, which has a mass-dependent magnitude, and hence a mass-dependent rate of background events. Our recovered joint posterior on  $\lambda$  and the Hubble constant is shown in Figure 5. This number of well localized and heavy events is expected to be available after  $\sim 2$  yr of LIGO/Virgo/KAGRA run at the sensitivity expected for O4, and, as already clear from the results of Section 4, it is expected to place a significant constraint on  $\lambda$  as long as  $\lambda > 0.1$ . For a true fraction of BBH in AGNs of  $\lambda = 0.6$ , after marginalizing over the true value of  $\lambda$ , the expected precision on  $H_0$  from 10 events is  $\sim 12\%$ .

## 6. Conclusions

In this Letter we show a statistical approach to measure the fraction of GW BBH mergers that induce AGN flares using BBH follow-up observations. First, we show that the AGN flare observed in coincidence with GW190521 is consistent with a background AGN flare, in other words, it is possibly uncorrelated with the GW event as the association cannot be made with confidence. We then show that follow-up campaigns of GW BBH events such as the one performed by ZTF for GW190521 can however effectively constrain the fraction of BBHs produced in AGNs, assuming that an electromagnetic counterpart can arise from the BBH, as predicted in McKernan et al. (2019). Assuming that counterpart candidates will be similar to the candidate in Graham et al. (2020) (or that more generic counterparts occur with a similar frequency in AGNs), and under conservative assumptions about the AGN number density, we find that follow-up campaigns of well-localized



BBH mergers will be much more effective at constraining the fraction of BBHs formed in AGNs than methods that do not rely on follow-up observations, and that a confident association could be already possible during the upcoming LIGO/Virgo/KAGRA run, O4. This is particularly important if multiple formation channels contribute to the observed GW BBH mergers (Zevin et al. 2020), i.e.,  $\lambda < 1$ . Even if  $\lambda \sim 0.1$ , following up  $\lesssim 10$  well-localized events will yield an informative measurement, whereas without follow-up, we would need  $10^3$ – $10^4$  events (which will not be available during O4).

We extend the formalism to measure cosmological parameters in the presence of signal and background flares. We show that this formalism can provide a joint posterior of the Hubble constant and  $\lambda$ . Assuming a flat  $\Lambda$ CDM cosmology with  $\Omega_m = 0.3$ , we recover a  $\sim 12\%$  precision on the Hubble constant from follow-up observations of 10 well-localized events. Future studies of these sources may also reveal interesting constraints on  $\Omega_m$  and the dark energy equation of state, given that the typical distances of the events considered are  $\gtrsim 1$  Gpc.

It is worth noting that the SF, which we use here, only quantifies the probability of a quasar luminosity excursion as a Gaussian variance, from which we compute a Gaussian probability. While this is more general than the use of Gaussians in a DRW model, the type of flare expected for this channel may not be well described by a Gaussian process. In the future, it will be interesting to empirically constrain the statistics of the specific flare expected from this BBH merger channel from a large AGN sample as in Graham et al. (2017), and then use that to derive a false-alarm probability and a constraint on  $\lambda$ . The method presented here is flexible enough so that a change of this kind can be easily incorporated.

We have applied the method presented to BBH in AGNs for current-generation GW detectors, but in the future it could also be interesting to apply this method to other kinds of possible BBH counterparts and to LISA massive black hole binaries, since similar conditions with several possible variable AGNs in the localization volume may occur.

We thank Zoltan Haiman, Imre Bartos, Doga Veske, Paul Martini, Saavik Ford, Robert Morgan, Marica Branchesi, Charlie Kilpartick, and Tamara Davis for very useful discussion on this topic. M.F. is supported by NASA through NASA Hubble Fellowship grant HST-HF2-51455.001-A awarded by the Space Telescope Science Institute. C.J.B. acknowledges support from the Illinois Graduate Survey Science Fellowship.

Work supported by the Fermi National Accelerator Laboratory, managed and operated by Fermi Research Alliance, LLC under Contract No. DE-AC02-07CH11359 with the U.S. Department of Energy. The U.S. Government retains and the publisher, by accepting the article for publication, acknowledges that the U.S. Government retains a non-exclusive, paid-up, irrevocable, world-wide license to publish or reproduce the published form of this manuscript, or allow others to do so, for U.S. Government purposes.

#### ORCID iDs

A. Palmese  <https://orcid.org/0000-0002-6011-0530>  
M. Fishbach  <https://orcid.org/0000-0002-1980-5293>  
C. J. Burke  <https://orcid.org/0000-0001-9947-6911>  
J. Annis  <https://orcid.org/0000-0002-0609-3987>  
X. Liu  <https://orcid.org/0000-0003-0049-5210>

#### References

- Abbott, B. P., Abbott, R., Abbott, T. D., et al. 2017a, *Natur*, 551, 85  
Abbott, B. P., Abbott, R., Abbott, T. D., et al. 2017b, *PhRvL*, 119, 141101  
Abbott, B. P., Abbott, R., Abbott, T. D., et al. 2018, *LRR*, 21, 3  
Abbott, B. P., Abbott, R., Abbott, T. D., et al. 2019, arXiv:1908.06060  
Abbott, R., Abbott, T., Abraham, S., et al. 2020b, *PhRvL*, 125, 101102  
Abbott, R., Abbott, T. D., Abraham, S., et al. 2020c, *ApJL*, 896, L44  
Abbott, R., Abbott, T. D., Abraham, S., et al. 2020d, arXiv:2010.14533  
Abbott, R., Abbott, T. D., Abraham, S., et al. 2020e, *ApJ*, 900, L13  
Abbott, R., Abbott, T. D., Abraham, S., Acernese, F., et al. 2020a, arXiv:2010.14527  
Ashton, G., Ackley, K., Hernandez, I. M., & Piotrzkowski, B. 2020, arXiv:2009.12346  
Baddeley, A., Rubak, E., & Turner, R. 2015, *Spatial Point Patterns: Methodology and Applications with R* (London: Chapman and Hall/CRC Press)  
Bartos, I., Haiman, Z., Marka, Z., et al. 2017a, *NatCo*, 8, 831, (B17)  
Bartos, I., Kocsis, B., Haiman, Z., & Márka, S. 2017b, *ApJ*, 835, 165  
Bellm, E. C., Kulkarni, S. R., Graham, M. J., et al. 2018, *PASP*, 131, 018002  
Berman, M. 1986, *J. R. Stat. Soc. Ser. C*, 35, 54  
Bouffanais, Y., Mapelli, M., Santoliquido, F., et al. 2021, arXiv:2102.12495  
Bustillo, J. C., Sanchis-Gual, N., Torres-Forné, A., et al. 2021, *PhRvL*, 126, 081101  
Chen, H.-Y., Fishbach, M., & Holz, D. E. 2018, *Natur*, 562, 545  
Chen, H.-Y., Haster, C.-J., Vitale, S., Farr, W. M., & Isi, M. 2020, arXiv:2009.14057  
Conselice, C. J., Bhatawdekar, R., Palmese, A., & Hartley, W. G. 2020, *ApJ*, 890, 8  
De Paolis, F., Nucita, A. A., Strafella, F., Licchelli, D., & Ingrassio, G. 2020, arXiv:2008.02692  
Del Pozzo, W. 2012, *PhRvD*, 86, 043011  
Djorgovski, S. G., Drake, A. J., Mahabal, A. A., et al. 2011, arXiv:1102.5004  
Farrell, E. J., Groh, J. H., Hirschi, R., et al. 2020, arXiv:2009.06585  
Fishbach, M., Gray, R., Magaña Hernandez, I., et al. 2018, arXiv:1807.05667  
Fishbach, M., & Holz, D. E. 2020, arXiv:2009.05472  
Fishbach, M., Holz, D. E., & Farr, B. 2017, *ApJL*, 840, L24  
Flesch, E. W. 2019, arXiv:1912.05614  
Ford, K. E. S., & McKernan, B. 2019, *MNRAS*, 490, L42  
Foreman-Mackey, D., Agol, E., Ambikasaran, S., & Angus, R. 2017, *AJ*, 154, 220  
Fragione, G., Loeb, A., & Rasio, F. A. 2020, arXiv:2009.05065  
Gayathri, V., Healy, J., Lange, J., et al. 2020a, arXiv:2009.05461  
Gayathri, V., Healy, J., Lange, J., et al. 2020b, arXiv:2009.14247  
Gerosa, D., & Berti, E. 2017, *PhRvD*, 95, 124046  
Graham, M. J., Djorgovski, S. G., Drake, A. J., et al. 2017, *MNRAS*, 470, 4112  
Graham, M. J., Ford, K. E. S., McKernan, B., et al. 2020, *PhRvL*, 124, 251102, (G20)  
Hao, L., Strauss, M. A., Fan, X., et al. 2005, *AJ*, 129, 1795  
Haster, C.-J. 2020, *RNAAS*, 4, 209  
Holz, D. E., & Hughes, S. A. 2005, *ApJ*, 629, 15  
Hopkins, P. F., Richards, G. T., & Hernquist, L. 2007, *ApJ*, 654, 731  
Kasliwal, V. P., Vogeley, M. S., & Richards, G. T. 2015, *MNRAS*, 451, 4328  
Kelly, B. C., Bechtold, J., & Siemiginowska, A. 2009, *ApJ*, 698, 895  
Kimura, S. S., Murase, K., & Bartos, I. 2021, arXiv:2103.02461  
Kimura, Y., Yamada, T., Kokubo, M., et al. 2020, *ApJ*, 894, 24  
Kinugawa, T., Nakamura, T., & Nakano, H. 2020, arXiv:2009.06922  
Kool, E. C., Reynolds, T. M., Mattila, S., et al. 2020, *MNRAS*, 498, 2167  
Kozłowski, S. 2016, *ApJ*, 826, 118  
LIGO Scientific Collaboration, & Virgo Collaboration 2019, GCN, 24621, 1  
LIGO Scientific Collaboration 2018, LIGO Algorithm Library—LALSuite, free software (GPL), <https://doi.org/10.7935/GT1W-FZ16>  
Luca, V. D., Desjacques, V., Franciolini, G., Pani, P., & Riotto, A. 2020, arXiv:2009.01728  
Mandel, I., Farr, W. M., & Gair, J. R. 2018, arXiv:1809.02063  
Masci, F. J., Laher, R. R., Rusholme, B., et al. 2018, *PASP*, 131, 018003  
McKernan, B., Ford, K. E. S., Bartos, I., et al. 2019, *ApJL*, 884, L50  
McKernan, B., Ford, K. E. S., Bellovary, J., et al. 2018, *ApJ*, 866, 66  
McKernan, B., Ford, K. E. S., Kocsis, B., Lyra, W., & Winter, L. M. 2014, *MNRAS*, 441, 900  
McKernan, B., Ford, K. E. S., Lyra, W., & Perets, H. B. 2012, *MNRAS*, 425, 460  
Morgan, R., Bechtol, K., Kessler, R., et al. 2019, *ApJ*, 883, 125  
Mukherjee, S., Ghosh, A., Graham, M. J., et al. 2020, arXiv:2009.14199  
Palmese, A., & Conselice, C. J. 2021, *PhRvL*, 126, 181103  
Palmese, A., deVicente, J., Pereira, M. E. S., et al. 2020, *ApJL*, 900, L33

- Palmese, A., Graur, O., Annis, J. T., et al. 2019, *BAAS*, **51**, 310
- Planck Collaboration, Aghanim, N., Akrami, Y., et al. 2018, arXiv:1807.06209
- Romero-Shaw, I. M., Lasky, P. D., Thrane, E., & Bustillo, J. C. 2020, arXiv:2009.04771
- Safarzadeh, M., & Haiman, Z. 2020, arXiv:2009.09320
- Schutz, B. F. 1986, *Natur*, **323**, 310
- Shen, X., Hopkins, P. F., Faucher-Giguère, C.-A., et al. 2020, *MNRAS*, **495**, 3252
- Singer, L. P., Chen, H.-Y., Holz, D. E., et al. 2016a, *ApJ*, **829**, L15
- Singer, L. P., Chen, H.-Y., Holz, D. E., et al. 2016b, *ApJS*, **226**, 10
- Singer, L. P., & Price, L. R. 2016, *PhRvD*, **93**, 024013
- Smith, K. L., Mushotzky, R. F., Boyd, P. T., et al. 2018, *ApJ*, **857**, 141
- Soares-Santos, M., Palmese, A., et al. 2019, *ApJL*, **876**, L7
- Tagawa, H., Haiman, Z., & Kocsis, B. 2020, *ApJ*, **898**, 25
- Urry, C. M., & Padovani, P. 1995, *PASP*, **107**, 803
- Wong, K. W. K., Breivik, K., Kremer, K., & Callister, T. 2020, arXiv:2011.03564
- Yang, Y., Bartos, I., Gayathri, V., et al. 2019, *PhRvL*, **123**, 181101
- Yang, Y., Gayathri, V., Bartos, I., et al. 2020, *ApJL*, **901**, L34
- Zevin, M., Bavera, S. S., Berry, C. P. L., et al. 2020, arXiv:2011.10057